Commissioning of the Cosmic Ray Tagger and measurement of its veto efficiency on the selection of contained neutrino interactions in SBND

INTERN Annalea Corallo *†
SUPERVISORS Michelle Stancari, Henry Lay

Abstract

During my internship at Fermilab, I contributed to the commissioning of the Cosmic Ray Tagger (CRT) system for the Short-Baseline Near Detector (SBND), part of the Short-Baseline Neutrino (SBN) Program. The CRT is a crucial component for identifying and vetoing cosmic ray events, improving the purity of neutrino data. My work primarily focused on the assembly and commissioning of the upper CRT layers (CRT Top Low and CRT Top High), where I tested and validated the cable delays and signal integrity, ensuring accurate time synchronization across the system. I also engaged in software activities, analyzing data from the CRT, including debugging the West Wall's anomalous high cosmic ray rate and validating the time signals in the Top High layer. Furthermore, I calculated the CRT's veto efficiency, which reached approximately 98%, demonstrating the system's excellent performance in detecting cosmic ray events during neutrino interactions. This experience provided hands-on training in both hardware and data analysis, solidifying the operational integrity of the CRT for SBND.

1 The Short-Baseline Neutrino Program

The Short-Baseline Neutrino (SBN) Program is a comprehensive experimental initiative based at Fermilab, aimed at investigating some of the most fundamental questions about neutrinos physics. The SBN Program uses the Booster Neutrino Beam (BNB) at Fermilab, which produces a beam of neutrinos by colliding protons with a target, creating pions and kaons that decay into neutrinos. These neutrinos then travel through a series of detectors placed at different distances along the beamline (see figure 1), enabling precise measurements of neutrino - Argon interactions.

There are three detectors in the SBN Program, all using liquid argon time projection chamber (LArTPC) technology, known for its excellent capability to reconstruct detailed images of particle interactions.[3] These detectors are:

- **SBND** (Short-Baseline Near Detector), located 110 meters from the neutrino source, designed to study the beam's composition before any oscillations occur.
- **MicroBooNE**, placed 470 meters from the source, which has been operational since 2015 and focuses on understanding neutrino interactions in liquid argon.
- **ICARUS**, the farthest detector at 600 meters, which was previously used in the Gran Sasso Laboratory in Italy and was refurbished for this experiment.

Together, these three detectors are arranged along the same beamline to provide a way to look for neutrino oscillations, i.e. changes in neutrino flavor as they travel, which would be indicative of new physics. By comparing the number of neutrinos detected at each stage, the program seeks to observe whether neutrinos are disappearing or transforming into other types, which would signal an anomaly beyond the current Standard Model of particle physics.[1]

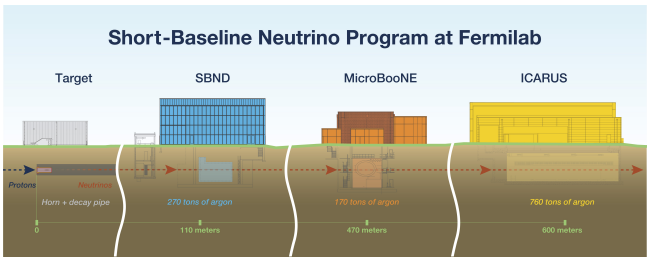

Figure 1: Layout of the three liquid argon time projection chambers (LArTPCs) in the Short-Baseline Neutrino Program: SBND (closest to the neutrino source), MicroBooNE, and ICARUS.

As a matter of fact, the primary scientific goal of the SBN Program is to resolve the LSND anomaly, a past observation suggesting the existence of a sterile neutrino. By studying the rate at which neutrinos oscillate between different flavors, the SBN Program hopes to provide definitive answers. The use of three detectors at varying distances from the source enables a sensitive search for such oscillations over a short baseline, optimizing the chances of identifying any deviations from the expected neutrino behavior.

In addition to its primary goal of searching for sterile neutrinos, the SBN Program will contribute to a broader understanding of neutrino physics. It will gather valuable data on neutrino interactions with matter, improve techniques for neutrino detection, and provide insights that could be applied to future neutrino experiments, such as the Deep Underground Neutrino Experiment (DUNE).

2 Short Baseline Near Detector

The Short-Baseline Near Detector (SBND) is the closest of the three detectors in the SBN Program at Fermilab, located just 110 meters from the neutrino source. Its primary role is to measure the unoscillated composition of the Booster Neutrino Beam, providing essential data on the beam's flux and interaction characteristics before neutrino oscillations can occur.
SBND consists of three main subsystems that allow it to capture and analyze neutrino interactions with unprecedented precision (see figure 2).

The core of SBND is its 112-ton active volume **liquid argon time projection chamber**. LArTPC technology is renowned for its ability to produce high-resolution 3D images of particle tracks. When neutrinos interact with argon atoms inside the detector, they produce charged particles that ionize the argon. These ionization

* *Univeristà degli Studi di Ferrara*
† annalea.corallo@gmail.com

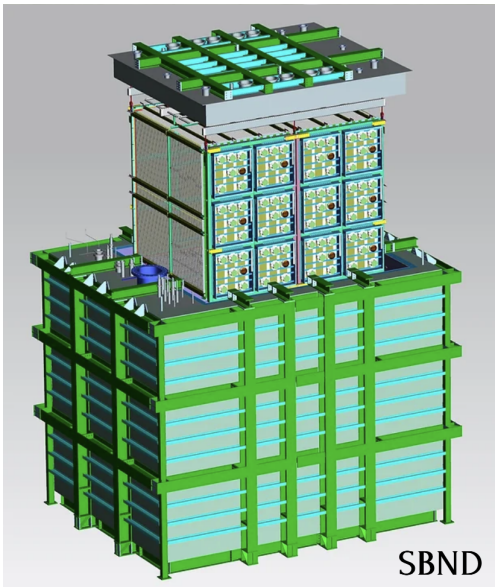

Figure 2: Internal structure of SBND, showing the liquid argon time projection chamber at the core, surrounded by the photon detection system, and encapsulated by the Cosmic Ray Tagger.

electrons drift through the chamber under the influence of an electric field, and their signals are captured by wire planes at the end of the chamber. The anode wire planes in SBND's LArTPC are composed of three planes of wires, each arranged at different angles relative to each other. This configuration enhances the ability to precisely reconstruct the three-dimensional tracks of particles. The wire planes are arranged as follows:

- the first plane is oriented at +60° relative to the vertical,
- the second plane is oriented at -60° relative to the vertical,
- the third plane is aligned vertically

When the ionization electrons reach the wire planes, they induce signals on the wires. These signals are read out to provide 2D projections of the particle tracks. By combining the signals from all three wire planes, a full 3D image of the particle trajectories can be reconstructed. This system allows for detailed event reconstruction with high spatial resolution, crucial for distinguishing different particle types and interaction modes.
SBND is equipped with a sophisticated **photon detection system** to complement the LArTPC. When neutrinos interact in liquid argon, they not only ionize the atoms but also produce flashes of light (scintillation). The PDS is designed to detect this light, allowing for accurate timing information of each interaction. The photon detection system in SBND is composed of two main components: photomultiplier tubes, **PMTs** and **X-ARAPUCA** light collectors. PMTs are placed behind the anode planes and are responsible for detecting the fast scintillation light that is produced almost instantaneously when a neutrino interacts with the liquid argon. PMTs are highly sensitive detectors that convert light into electrical signals via the photoelectric effect, amplifying the signal to provide precise timing information. The scintillation light serves as a timing reference, allowing for accurate reconstruction of the drift time of ionization electrons, which is essential for determining the location of the interaction within the LArTPC. This also helps in identifying background events and distinguishing neutrino interactions.
The X-ARAPUCA is an advanced light-collection technology that complements the PMTs. X-ARAPUCAs are placed within the detector to capture and enhance the detection of scintillation light. The system works by trapping photons inside a small, highly reflective cavity. It uses a dichroic filter that allows light to enter but not escape, effectively capturing photons and guiding them towards a silicon photomultiplier (SiPM). This setup increases the efficiency of light collection, particularly for the scintillation light in the vacuum ultraviolet (VUV) range produced by liquid argon. X-ARAPUCAs are extremely efficient in collecting light over a large area, ensuring that even low-energy events are captured, which improves the detector's overall sensitivity and timing resolution.
Being located near the Earth's surface means that SBND is exposed to a significant flux of cosmic rays, which can mimic neutrino interactions and lead to background noise in the data. To mitigate this, SBND is equipped with a comprehensive **cosmic ray tagger** (CRT) system [2.1]. The CRT surrounds the detector and acts as a veto system, identifying cosmic rays as they pass through or near the detector. By tagging and excluding these cosmic events, the CRT helps ensure that the data collected is predominantly due to neutrino interactions, thereby improving the overall purity of the dataset. This is particularly important for enhancing the sensitivity of the search for neutrino oscillations.[2]
SBND's position just 110 meters from the BNB source is a significant advantage. Due to its proximity, the detector experiences a very high neutrino flux, meaning a large number of neutrino interactions occur within the detector each year. This high interaction rate allows SBND to gather large amounts of data in a relatively short period of time, significantly reducing statistical uncertainties in measurements. Moreover, since SBND is located before neutrino oscillations have taken place, it provides a "baseline" measurement of the beam composition, which is essential for comparing with the results from the downstream detectors, MicroBooNE and ICARUS. It is estimated that the detector will observe approximately 1.5 million neutrino interactions per year. This high event rate is crucial not only for studying the detailed characteristics of neutrino interactions but also for serving as a reference point for oscillation analyses. By comparing SBND's measurements with those from the farther detectors, researchers can precisely study how the neutrino composition changes as the neutrinos travel.
In summary, SBND is a critical component of the SBN Program, its LArTPC provides high-resolution imaging of neutrino interactions, the photon detection system adds precise timing information, and the cosmic ray tagger ensures data purity by filtering out background events. With its close proximity to the BNB, SBND's high neutrino flux enables it to collect extensive data, making it an invaluable asset in the search for new physics beyond the Standard Model.

2.1 Cosmic Ray Tagger

The Cosmic Ray Tagger (CRT) of SBND consists of seven scintillator modules, arranged with six in a cube formation around the detector and an additional layer on top. Each of these modules is made up of two perpendicular layers, referred to as the X and Y layers (see figure 3).

These layers are composed of scintillator slabs, within which there are 16 scintillator strips. Each strip is read out by 32 silicon photomultipliers (SiPMs). A signal is produced when at least two

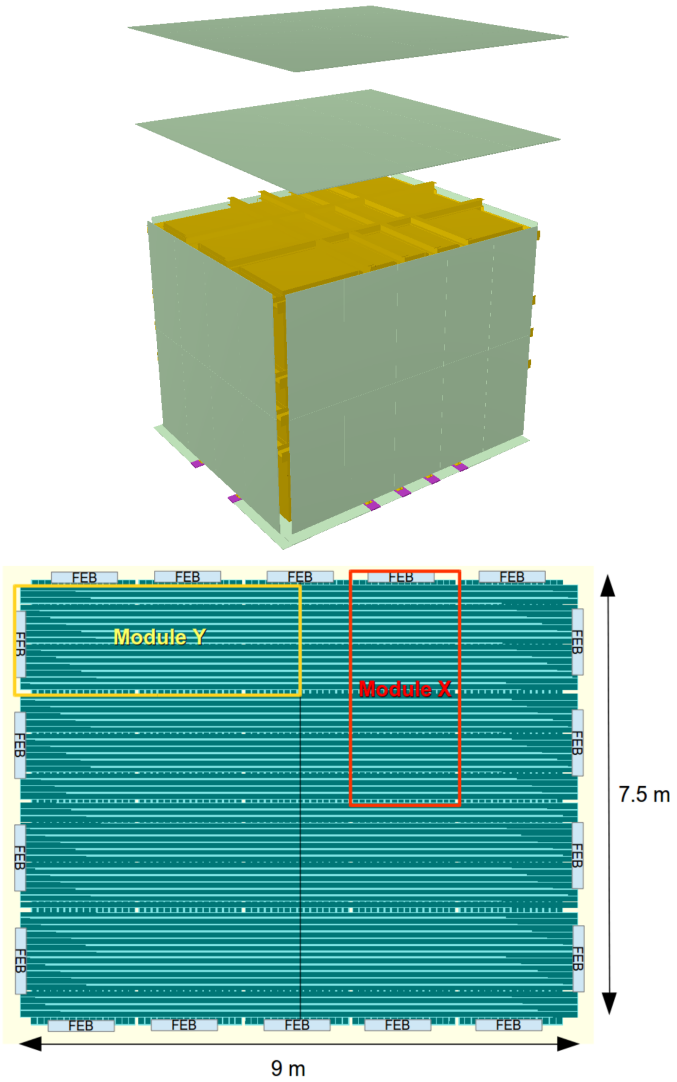

Figure 3: The figure above shows the geometric arrangement of the seven SBND CRT modules. Each module contains two perpendicular layers X and Y, as shown in the figure below.

of the SiPMs in a slab detect a signal above a preset threshold.

To confirm that a particle has passed through the detector, the system requires a coincidence between the signals from the X and Y layers within a short time window. This process ensures that the event corresponds to an actual particle crossing the detector rather than background noise 4.

The signals from each module are read by front-end electronic boards (FEBs), which are responsible for processing and forwarding the data. Each FEB receives four timing pulses: T0, i.e. the reference time from a GPS system known as PPS, T1, i.e. a signal alerting the detector when a neutrino beam is incoming, T_{in} and T_{out}, i.e. the input and output signals that allow the daisy-chaining of multiple modules (as shown in figure 5).

This coincidence system is crucial for reducing background noise, ensuring that the detected signals are genuinely related to the passage of a particle, rather than false signals from environmental or instrumental noise. The modular design and layered arrangement allow for efficient cosmic ray detection, providing valuable data for

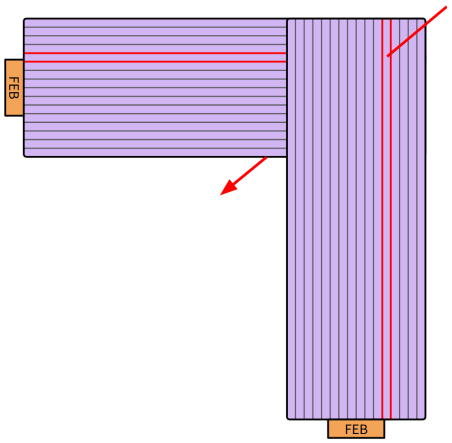

Figure 4: Illustration of signal production in the SBND CRT: when a particle passes through, two channels in one module register a signal, and a corresponding signal is detected in the perpendicular module, confirming the particle's trajectory through coincidence.

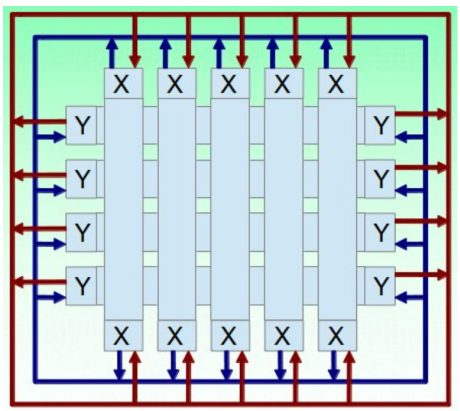

Figure 5: Illustration of the daisy chain connection between the X and Y layers of the SBND Cosmic Ray Tagger (CRT): each module's perpendicular layers are interconnected via the daisy chain, transmitting timing signals (T_{in} and T_{out}) and ensuring coordinated signal readout across the system for accurate particle detection.

the SBND experiment.

3 Hardware activities

A significant part of my internship at Fermilab was focused on hardware activities, particularly in assembling and commissioning the upper layers of the Cosmic Ray Tagger. Specifically, I worked on the CRT Top Low and CRT Top High layers. This involved hands-on participation in the integration and placement of scintillator modules, ensuring that the detection system was properly aligned and functioning. Additionally, I collaborated with other members of the CRT group to connect all the cables between the modules and properly ground them to the detector ground.

3.1 CRT Top Low commissioning

In the initial weeks of my internship, my role primarily involved verifying the proper delay of all cables that were later installed, utilizing an oscilloscope and a waveform generator to ensure that

the signal waveform was not altered. Once each cable was tested, it was labeled to indicate its installation location, and colored tape was applied to differentiate the cables corresponding to the four different time signals. On August 13th, the installation and validation of the CRT Top Low were completed (see figure 6). As refernce, in figure 7 is shown the apparatus status before the installation of the CRT Top Low and Top High layers.

Figure 6: Image showing the Top Low layer of the Cosmic Ray Tagger.

Figure 7: Photo of the initial state of the detector before the installation of the Top Low and Top High layers of the Cosmic Ray Tagger.

3.2 CRT Top High commissioning

In the second part of my internship, I focused on the commissioning of the Top High layer of the CRT. The activities involved were the same as those required for the installation of the CRT Top Low, including testing the cable delays and signal shapes, labeling each cable with colors and tags. Unlike the Top Low layer, the installation of the cables for the CRT Top High also required the use of a basket (as shown in figure 8), operated by specialized personnel, to access the FEBs in the central, north, and south regions of the CRT.

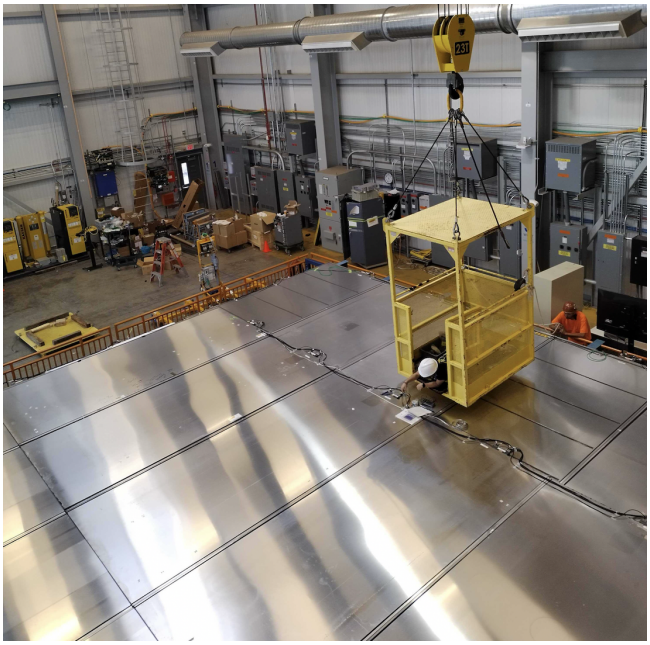

Figure 8: Photo of me working from the basket to ground the modules of the CRT Top High.

In addition to connecting the cables to the various FEBs, grounding of the different modules was also performed. The installation of the layer was completed one month after the installation of the CRT Top Low, on September 13th (see figure 9).

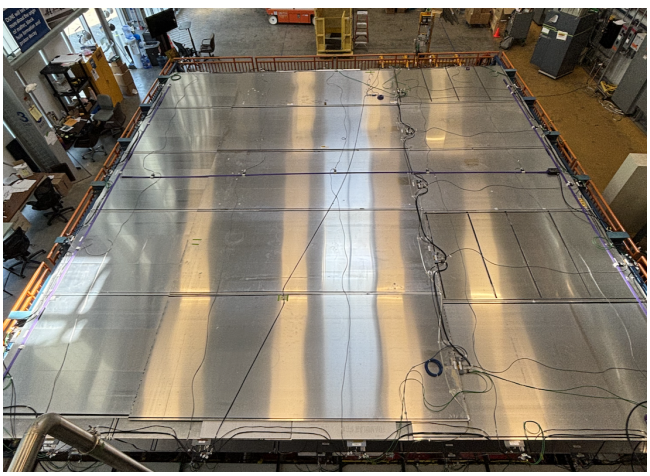

Figure 9: Photo of the completed CRT Top High layer.

4 Software and data analysis activities

Alongside my hardware activities during the internship, I also had the opportunity to analyze some of the data from SBND. Specifi-

cally, I focused on three main tasks: first, I worked on resolving the issue related to the rate of the West Wall, which required direct intervention on the connections of the FEBs; second, I validated the time signals from the initial runs of the CRT Top High acquisition to ensure that the installation of all the cables had been executed correctly; and finally, I calculated the veto efficiency of the CRT in a contained neutrino event. For these tasks, I wrote scripts in ROOT, accessing the trees of the experiment to extract and analyze the relevant data.

4.1 Debugging of the West wall

During the first weeks of my internship, an unusually high rate of cosmic rays was observed in the West Wall, which had already been installed and validated. A possible cause for this anomaly could be a wrong connection between the T_{in} and T_{out} cables in the daisy chain of the wall. If these two cables are reversed, instead of obtaining two separate daisy chains, only a single chain is formed. The first step to verify this behavior involved using four spare FEBs and a multimeter to measure the resistance between the two FEB chains, both in the correct connection scenario and in the case where the wires were inverted. Upon checking the actual impedance recorded between the ends of the two chains in the West Wall of the CRT, we found a value consistent with the situation where the cables were incorrectly connected, resulting in a single daisy chain instead of two separate ones. To definitively confirm that the intervention was correct, three different runs were acquired before and after the cables were properly connected. Specifically, two plots were generated for each run: one showing the rate of recorded events and another displaying the ratio of space points to strip hits. Space points are generated only when there is an actual coincidence between the two perpendicular layers, while strip hits are signals associated with any signal generated in a given module, regardless of whether there is a coincidence in the perpendicular module. For a properly functioning system, we expect the ratio of space points to strip hits to be approximately 1.
The figure 10 shows that with subsequent interventions, the rate recorded by the individual modules has indeed decreased, approaching a value similar to that recorded by the other walls. Additionally, the ratio of space points to strip hits has converged towards 1. In the first run, due to the lack of separation between the two daisy chains, the modules of the perpendicular layers were not properly coupled, resulting in the absence of space points.

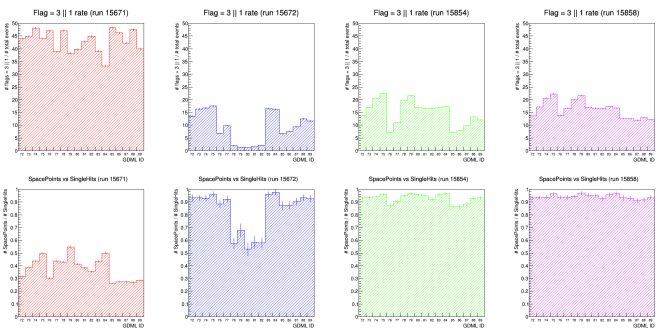

Figure 10: The top row displays the trend of the cosmic ray rate across the different modules of the West Wall throughout the various interventions. The second row shows the measured ratio between space points and strip hits.

As can be seen by observing the plot in the top row, the rate of observed cosmic rays decreases to a value more similar to that recorded by the other walls. Additionally, it can be noted that the distribution of rates reflects the physical arrangement of the modules.

In the first four bins, as well as in the second four, an increasing distribution can be observed: these modules correspond to the two groups of horizontal modules, starting with the one lower down, which records a lower rate, gradually increasing to the one positioned higher up.

In contrast, regarding the last groups of 5 bins, it is noted that within the individual groups, the rate remains fairly constant, while the rate recorded by the first group is greater than that recorded by the second. These groups correspond to the vertical modules, with the group with the higher rate corresponding to the group of vertical modules arranged in the upper row, while the one with the lowest rate corresponds to the one in the lower row. For a better visualization of the arrangement of the modules in space, please refer to figure 11.

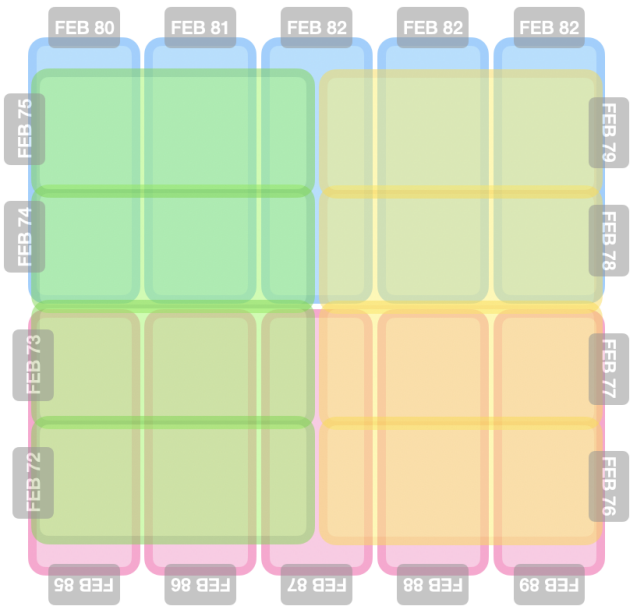

Figure 11: Schematic representation of the arrangement of the modules in the west wall, front view.

4.2 CRT Top High validation

The second part of my work focused on validating the timing signals of the CRT Top High after installation. To achieve this, I analyzed three different runs, each lasting approximately 20 minutes. The first run (number 16837) was acquired by sending the PPS signal to the T0 channel, while the fake beam signal—an initial pulse of about 50 ns within a 900 ns time window—was sent to the T1 channel. Two additional runs (numbers 16861 and 16903) were acquired by sending the PPS signal usually sent to T0 to T1, verifying the correct operation of the latter channel as well.

The first quantity analyzed was the value of the flags recorded during these acquisitions. The flag is an integer between 0 and 15 linked to a binary code: the ___x bit is 1 when the T0 signal is valid, the __x_ bit performs the same role for T1, the _x__ bit is 1 when the event corresponds to a reset signal of the T0 channel, and the x___ bit corresponds to a reset of T1. Therefore, for run 16837, the

expected flags were 0011, 0111, and 1011, thus corresponding to flag 3, 7 and 11 respectively. While for the swapped-signal runs, the expected flags were 0010 and 1010, corresponding to flag 2 and 10. The recorded values matched these expectations, as shown in Figure 12.

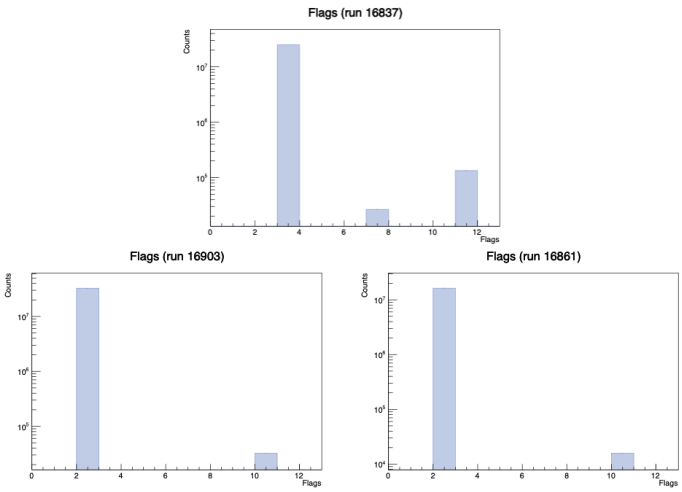

Figure 12: Plot of the flag values obtained during the three different runs.

After ensuring that the FEBs were correctly powered, it was important to verify that the four timing signals worked as expected. For the reference timing signals T0 and T1, two main analysis were performed. The first was to verify that the temporal distribution matched the signal sent to the detector. As seen in figures 13, 14, 15 and 16, 17, 18, the expected behavior was indeed observed during the different runs.

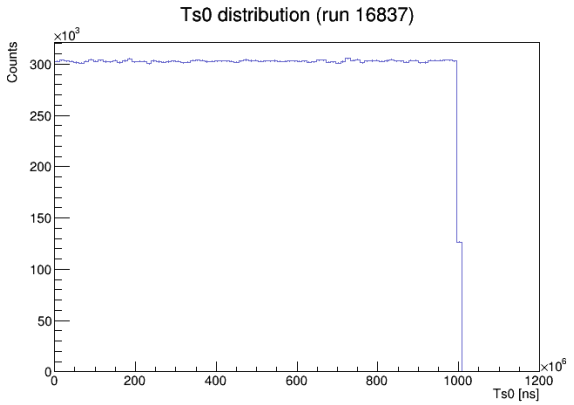

Figure 13: Plot of the T0 distribution in run 16837.

Another important quantity to evaluate was the clock drift, which is the precision with which the FEBs get the reset. To plot this, only reset events were selected. For run 16837, I chose T0 reset events with flag = 7, while for runs 16861 and 16903, I selected flag = 2 events for T1 validation. The clock drift was plotted by subtracting 1e9 ns (1 second, the expected reset time) from the time signal. A good clock drift corresponds to a narrow distribution centered around 0 s, which was observed for the T0 reset signal (Appendix A). For T1, however, the drift was narrowly

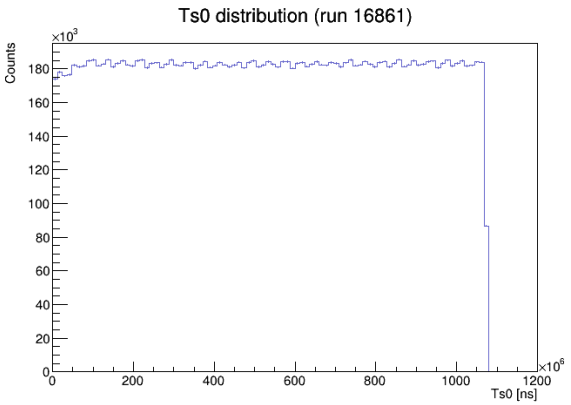

Figure 14: Plot of the T0 distribution in run 16861.

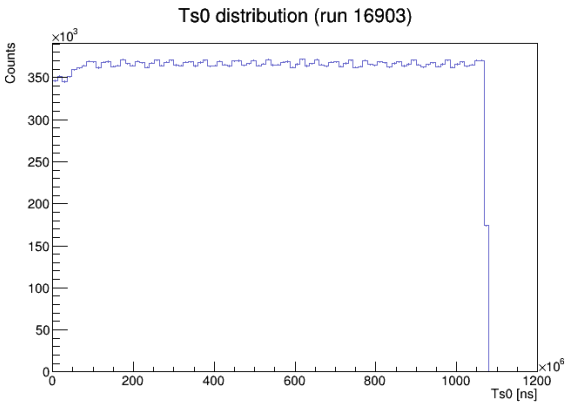

Figure 15: Plot of the T0 distribution in run 16903.

distributed but not centered at 0, instead showing random positive and negative values (Appendix B).

One possible cause for this behavior is that FEBs might struggle with the T1 signal if they do not receive a proper T0 signal. To test this hypothesis, a new run was performed where the PPS signal was sent to T0 (which previously had no reference signal) and a periodic signal, slightly phase-shifted from the PPS, was sent to T1. In this new configuration, plotting the T1 clock drift produced the expected zero-centered distribution, confirming the correct operation also of the T1 channel.

In addition to validating the T0 and T1 signals, the proper functioning of the T_{in} and T_{out} daisy chains needed to be verified. For this, I created a plot where each point corresponded to any coincidence in the readout of X and Y modules. In figure 19, distinct groups can be seen corresponding to the geometrical layout and overlap of the modules.

Modules with greater overlap (highlighted in green in figure 20) have a higher rate, partially overlapping modules show a lower rate (orange, figure 20), and modules with minimal overlap have the lowest rate (bordeaux, figure 20). Black points in the lower part of the graph represent coincidental readouts from non-overlapping X and Y modules. This correspondence between rate and module geometry confirms that the T_{in} and T_{out} chains are functioning correctly.

Following these analyses, it can be concluded that the Top High layer of the Cosmic Ray Tagger has been successfully installed and is operating as expected.

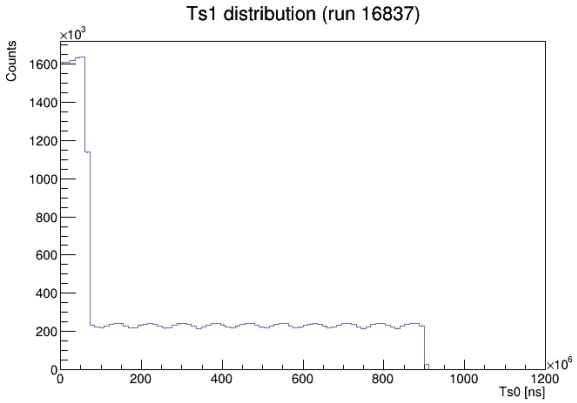

Figure 16: Plot of the T1 distribution in run 16837.

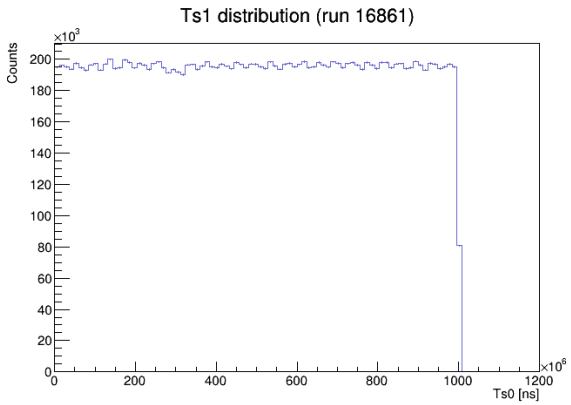

Figure 17: Plot of the T1 distribution in run 16861.

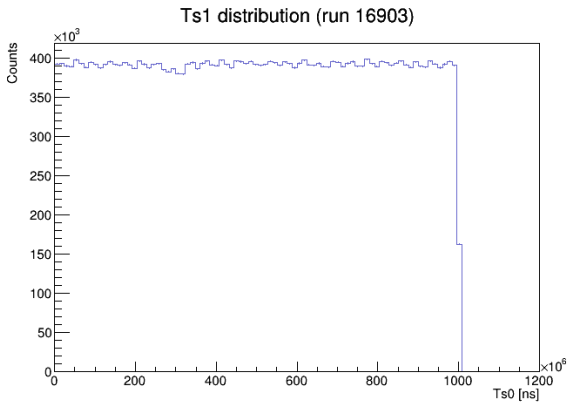

Figure 18: Plot of the T1 distribution in run 16903.

4.3 Measurement of the efficiency of using a CRT veto in a contained neutrino trigger

The final analysis I conducted involved calculating the CRT veto efficiency during a contained neutrino event, which is the probability that the CRT is not triggered during a neutrino event. To determine this value, the first step was to analyze the time distribution of events around the trigger signal. I plotted the timestamp value relative to the T0 reference signal, subtracting the trigger time in run 16906. As shown in Figure 21, the distribution is not

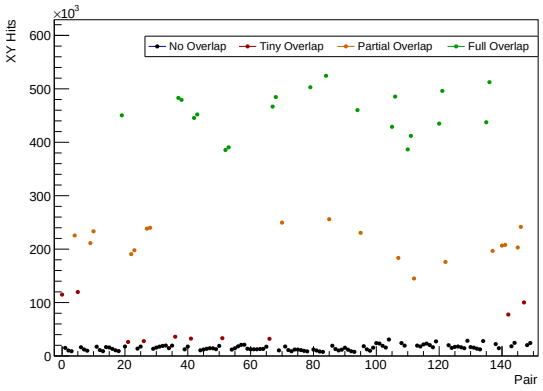

Figure 19: In this plot, each 3D point corresponds to any coincident readouts from both the X and Y modules.

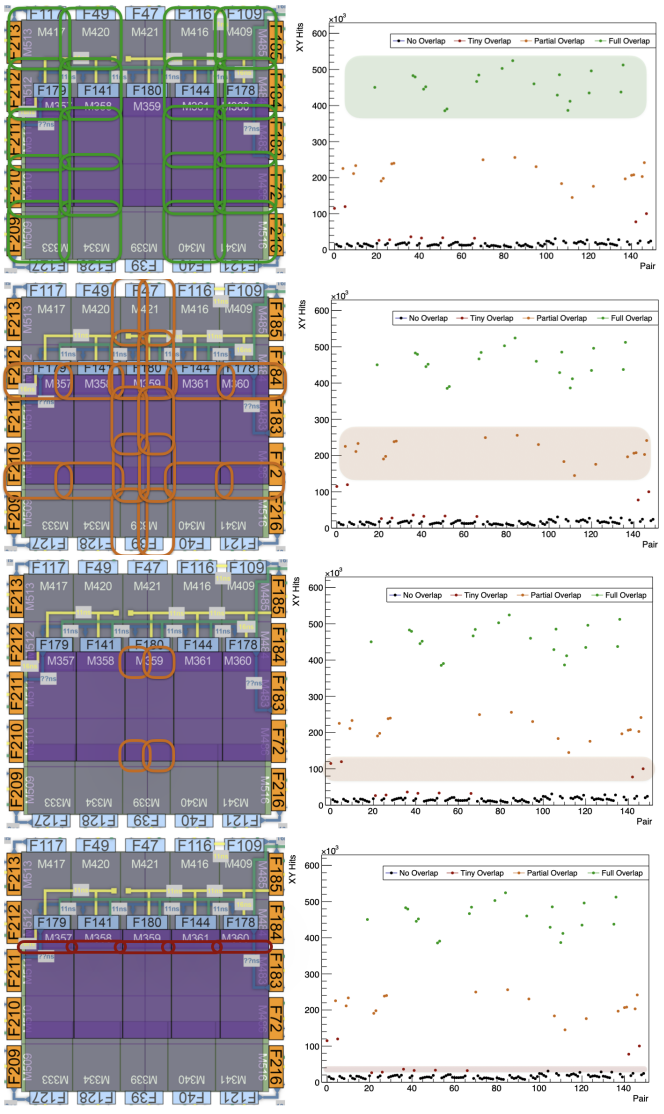

Figure 20: Image showing the correspondence between the rates and the geometric overlap of the different modules. From top to bottom, respectively: full, partial, minor partial and tiny overlaps.

uniform but rather trapezoidal in shape. For this reason, to calculate the veto efficiency, I considered only events recorded within a time window of ± 15 ms from the trigger signal to ensure all signals were being captured within a reliable region.

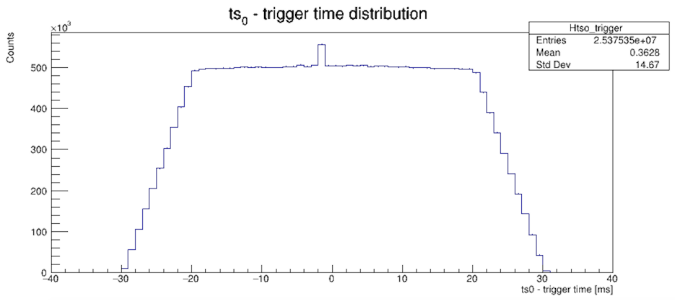

Figure 21: Time distribution of the signals with respect to the trigger time.

Next, I plotted the temporal distribution of events within this selected time window, as shown in figure 22.

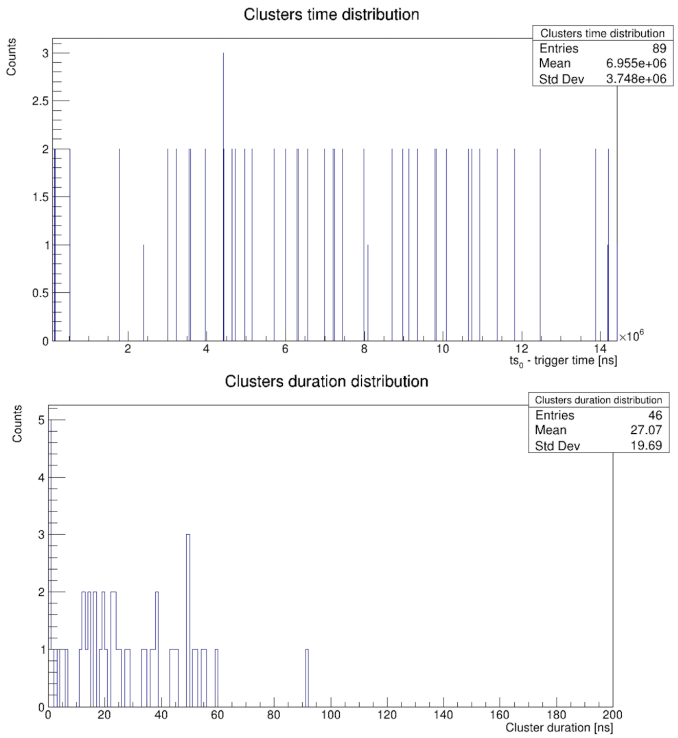

Figure 22: In the top image, the distribution of events corresponding to physical signals (flag = 3 [0011] indicating that the FEBs are receiving both T0 and T1 signals) within a trigger window is shown, with events clearly grouped into clusters. In the bottom image, the temporal distribution of events within one cluster is displayed, revealing that the events are grouped within a 200 ns window.

The signals appeared clustered into subgroups lasting a maximum of ~100 ns. Therefore, I treated all signals occurring within a 200 ns window from the first signal in each subgroup as a single event. Finally, I counted the 200 ns subgroups detected in each trigger window. This method allowed me to calculate an accurate estimate of the cosmic ray rate impacting the detector, based on the raw CRT data. Specifically, Figure 23 shows the distribution of the cosmic ray rate on the south, east, and Top Low walls of the CRT.

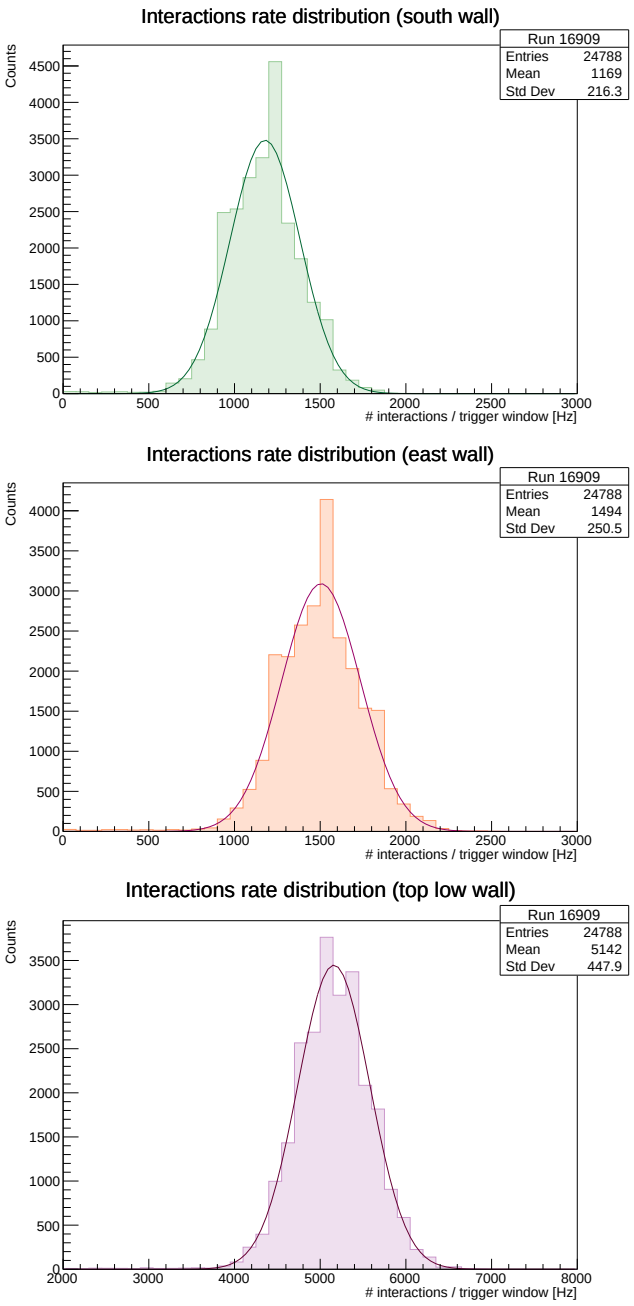

Figure 23: Distribution of the cosmic ray rate in the south, east, and Top Low walls of the Cosmic Ray Tagger.

The CRT veto efficiency can then be estimated assuming the cosmic ray rates on the various walls are as follows:

- South wall: 1150 Hz;
- North wall: 1300 Hz;
- East wall: 1500 Hz;
- West wall: 1500 Hz;

- Bottom wall: 2300 Hz;
- Top Low wall: 5150 Hz;
- Top High wall: 5150 Hz.

The overall cosmic ray rate on the detector results to be approximately 18000 Hz. Given that a neutrino beam spill lasts about 2 μs, the CRT veto efficiency, considering all the walls (including the Top High), is about 98%, demonstrating the high efficiency of the CRT's veto function.

5 Conclusion

My internship at Fermilab provided invaluable hands-on experience in both hardware and data analysis, contributing to the successful commissioning of the Cosmic Ray Tagger (CRT) for the Short-Baseline Near Detector (SBND). By assembling and validating the CRT's upper layers and analyzing its time signals, improving the system's efficiency and performance. The combination of these efforts resulted in a CRT veto efficiency of approximately 98%, significantly enhancing SBND's ability to discriminate between cosmic ray and neutrino events. This work contributes to SBND's goal of improving the precision in detecting neutrino oscillations and supports the overall scientific mission of the SBN Program. This experience not only deepened my understanding of detector technology and experimental physics but also equipped me with critical problem-solving skills in a large-scale research environment. It solidified my interest in particle physics and affirmed the importance of meticulous experimental validation in high-precision physics experiments.

Acknowledgments

I would like to express my sincere gratitude to Michelle Stancari for giving me the opportunity to join and work within a real research group.

A special thank you to Henry, your unwavering smile and positive attitude turned even the toughest challenges into opportunities for growth, and your trust gave me the confidence to push forward in every new task. Working alongside you was not only productive but genuinely fun, and for that, I am deeply grateful.

I would also like to thank the entire SBND CRT team, whose expertise and collaboration made this internship a success.

I also want to thank those who made this experience unforgettable outside the lab, especially Giulia and Mattia.

I am also grateful to those who made this experience possible from the very beginning: Prof. Calabrese, Prof. Tomassetti, Prof. Luppi, and Dr. Guarise. Finally, my recognition goes to INFN and the University of Pisa, who each year give students the opportunity to take part in this wonderful experience.

References

[1] R Acciarri, C Adams, R An, C Andreopoulos, AM Ankowski, M Antonello, J Asaadi, W Badgett, L Bagby, B Baibussinov, et al. A proposal for a three detector short-baseline neutrino oscillation program in the fermilab booster neutrino beam. *arXiv preprint arXiv:1503.01520*, 2015.

[2] Sergio Bertolucci, Dott Alessandro Montanari, and Francesco Poppi. The cosmic ray tagger of the short baseline neutrino experiment at fermilab.

[3] Carlo Rubbia. The liquid-argon time projection chamber: a new concept for neutrino detectors. Technical report, 1977.

A T0 clock drift plots

A.1 Run 16837

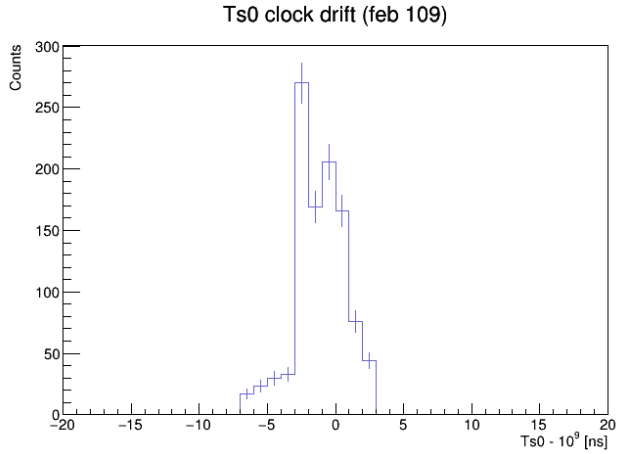

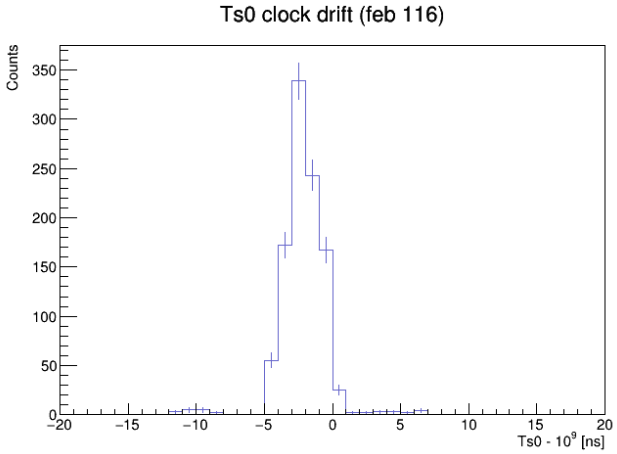

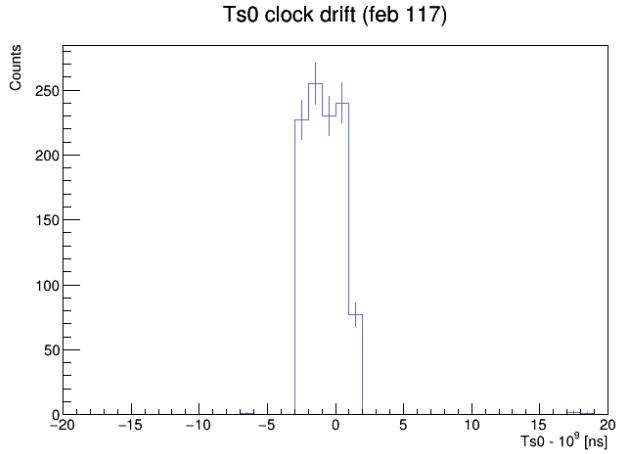

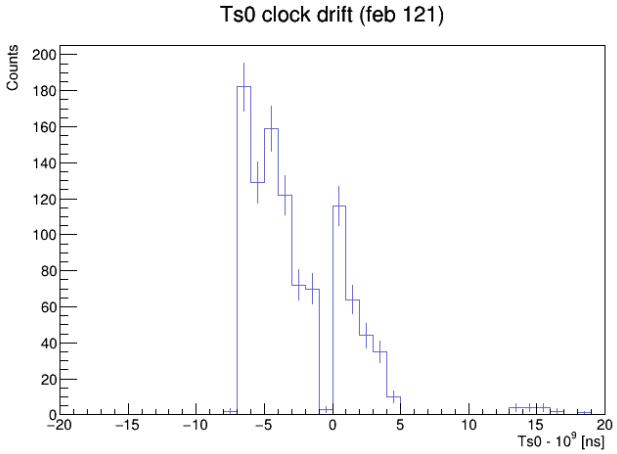

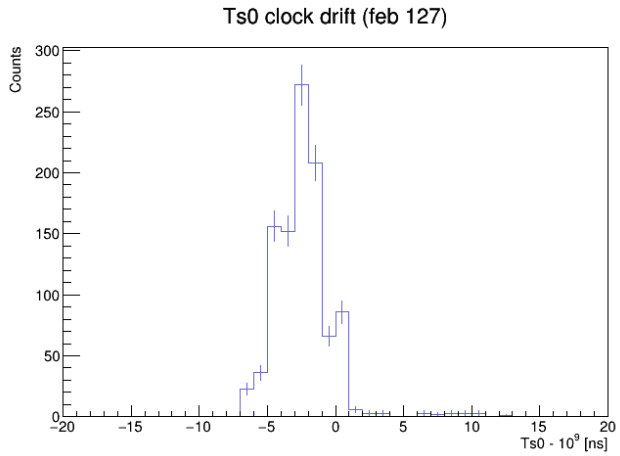

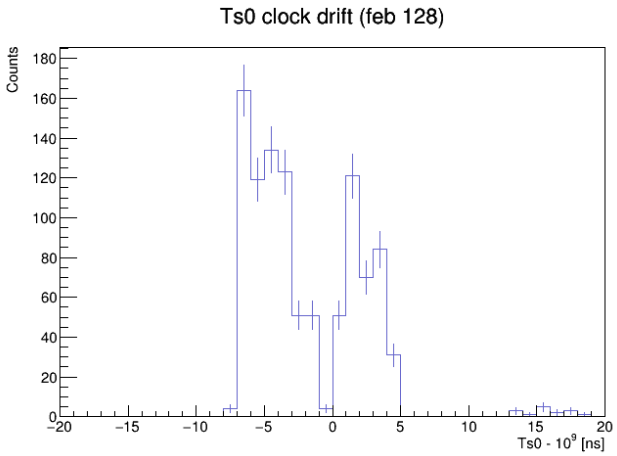

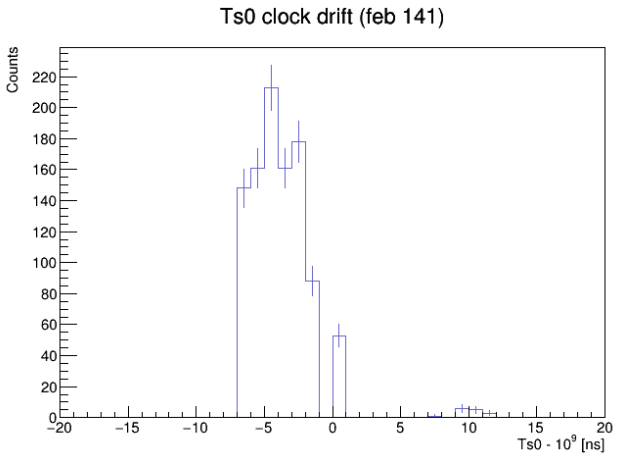
Ts0 clock drift (feb 141)
Counts
Ts0 - 10^9 [ns]

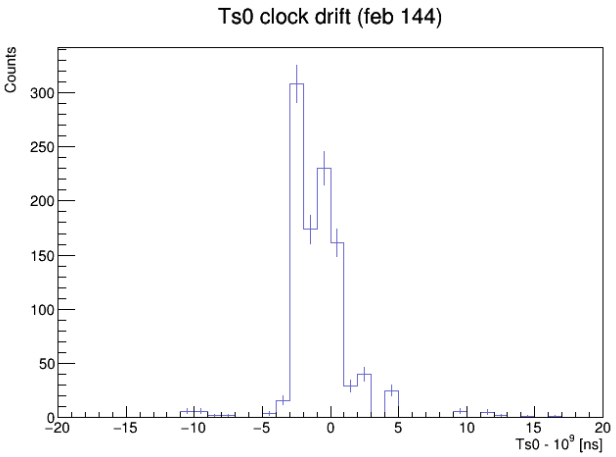
Ts0 clock drift (feb 144)
Counts
Ts0 - 10^9 [ns]

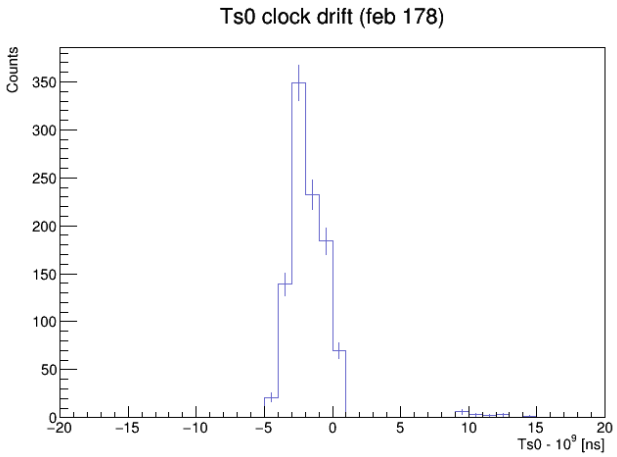
Ts0 clock drift (feb 178)
Counts
Ts0 - 10^9 [ns]

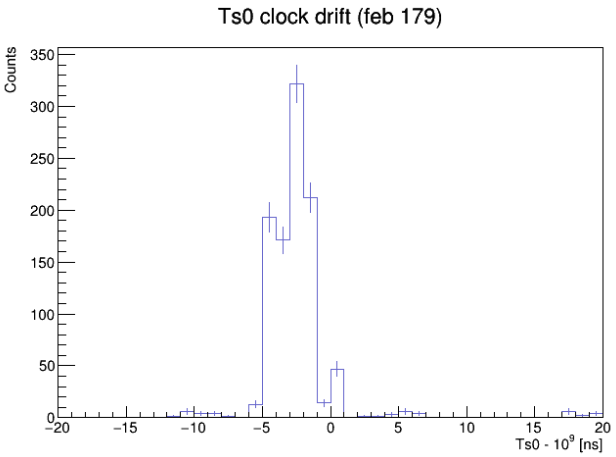
Ts0 clock drift (feb 179)
Counts
Ts0 - 10^9 [ns]

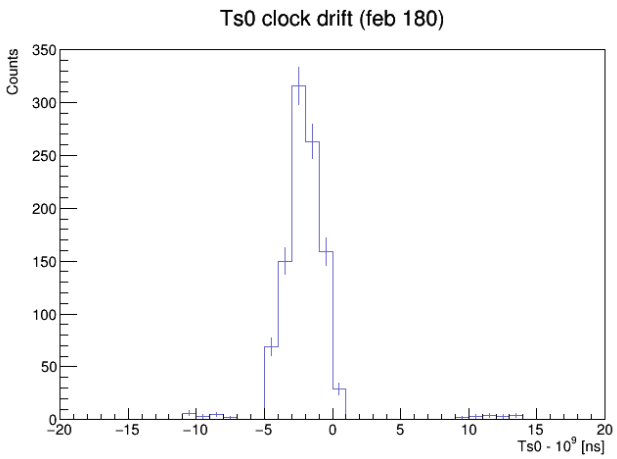
Ts0 clock drift (feb 180)
Counts
Ts0 - 10^9 [ns]

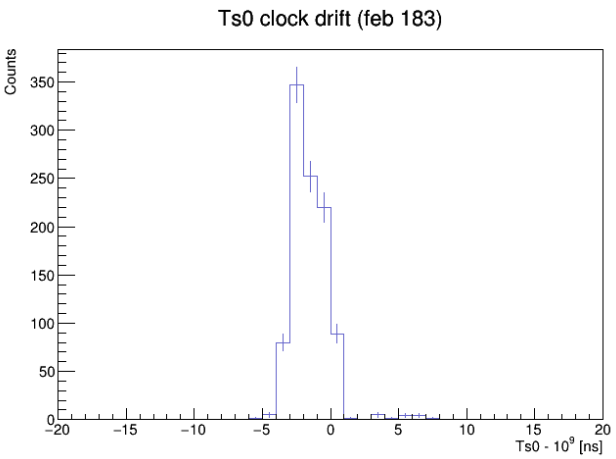
Ts0 clock drift (feb 183)
Counts
Ts0 - 10^9 [ns]

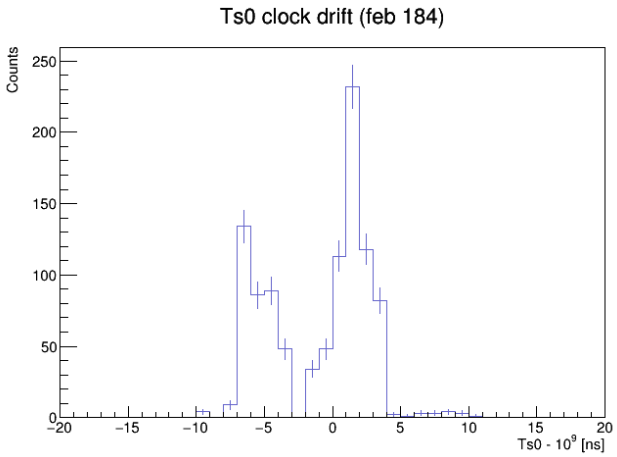
Ts0 clock drift (feb 184)
Counts
Ts0 - 10^9 [ns]

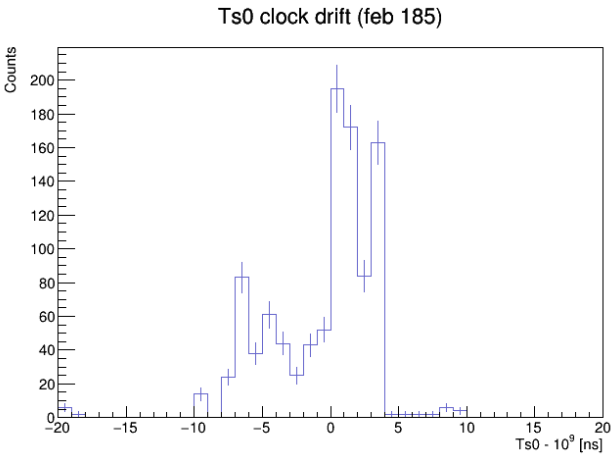
Ts0 clock drift (feb 185)
Counts
Ts0 - 10^9 [ns]

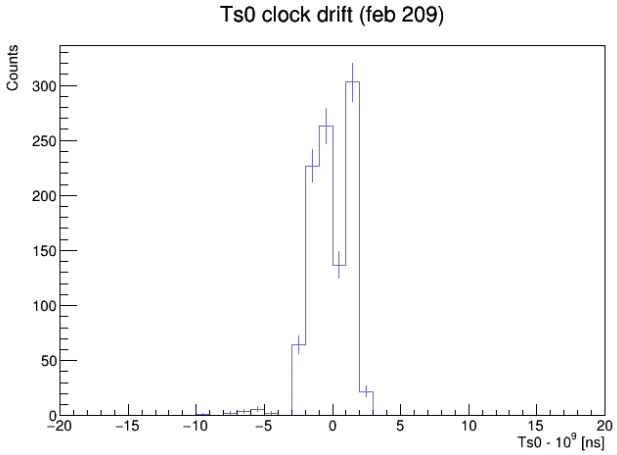
Ts0 clock drift (feb 209)
Counts
Ts0 - 10^9 [ns]

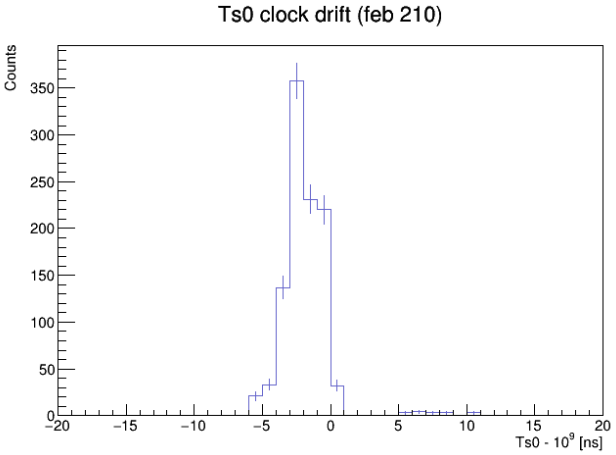
Ts0 clock drift (feb 210)
Counts
Ts0 - 10^9 [ns]

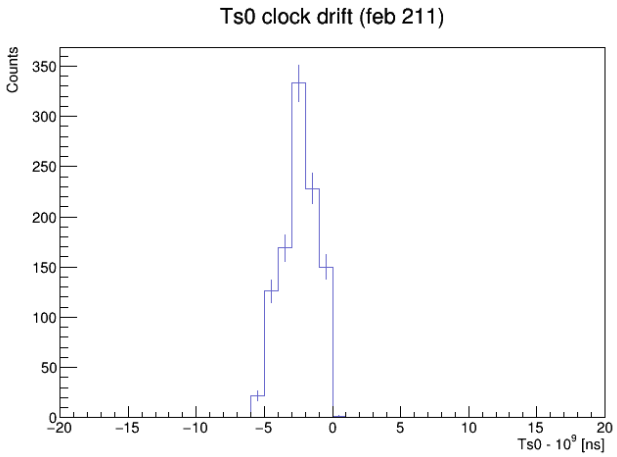
Ts0 clock drift (feb 211)
Counts
Ts0 - 10^9 [ns]

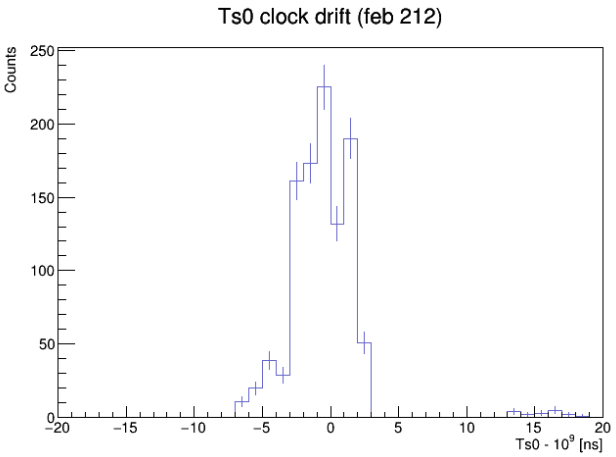
Ts0 clock drift (feb 212)
Counts
Ts0 - 10^9 [ns]

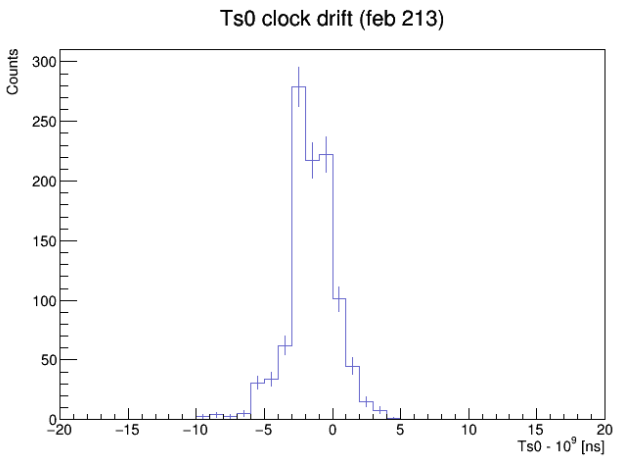
Ts0 clock drift (feb 213)
Counts
300
250
200
150
100
50
0
−20
−15
−10
−5
0
5
10
15
20
Ts0 - 10^9 [ns]

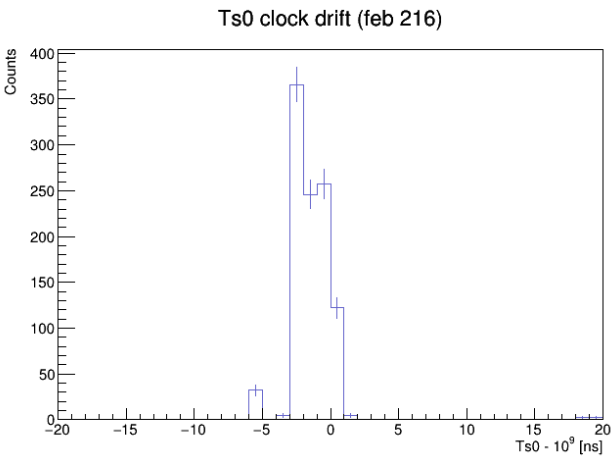
Ts0 clock drift (feb 216)
Counts
400
350
300
250
200
150
100
50
0
−20
−15
−10
−5
0
5
10
15
20
Ts0 - 10^9 [ns]

B T1 clock drift plots

B.1 Run 16861

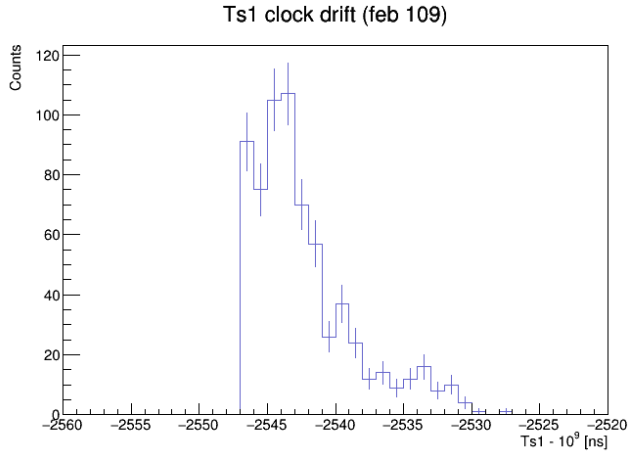

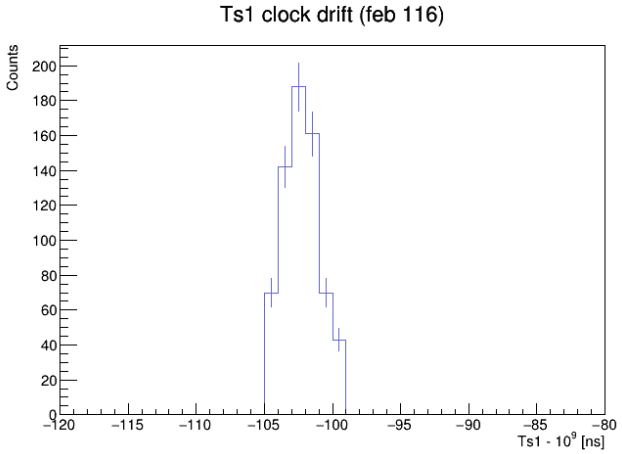

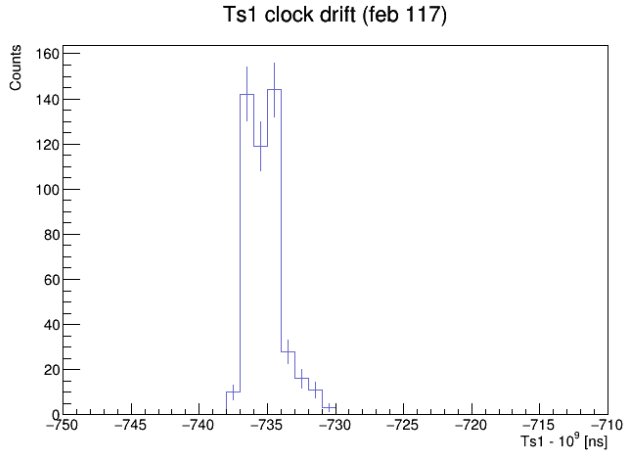

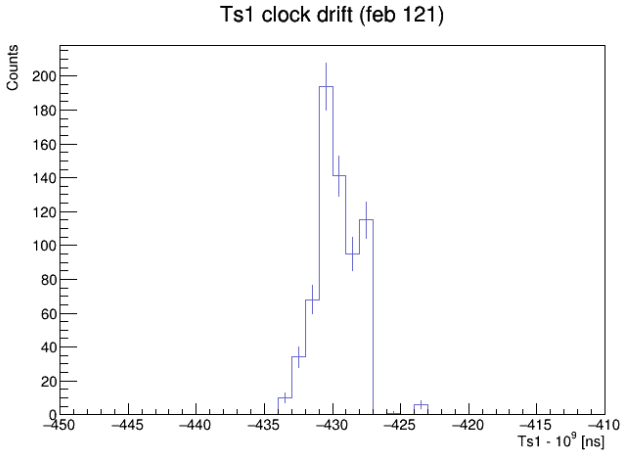

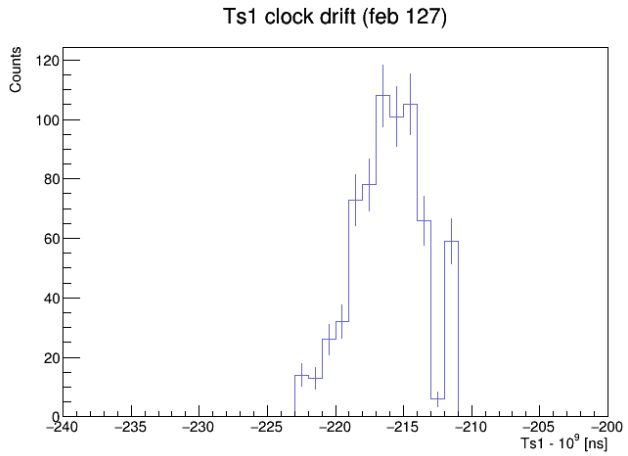

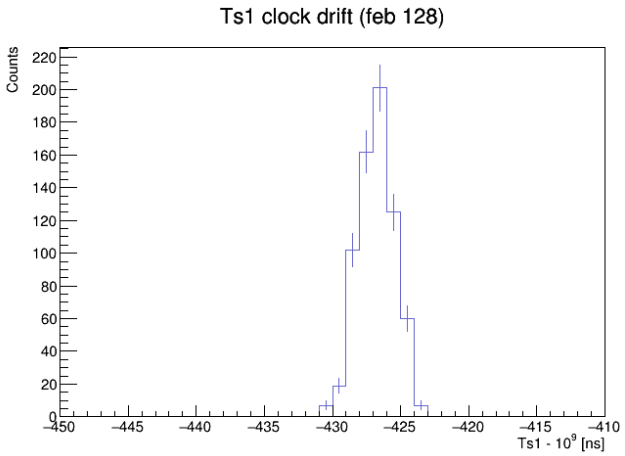

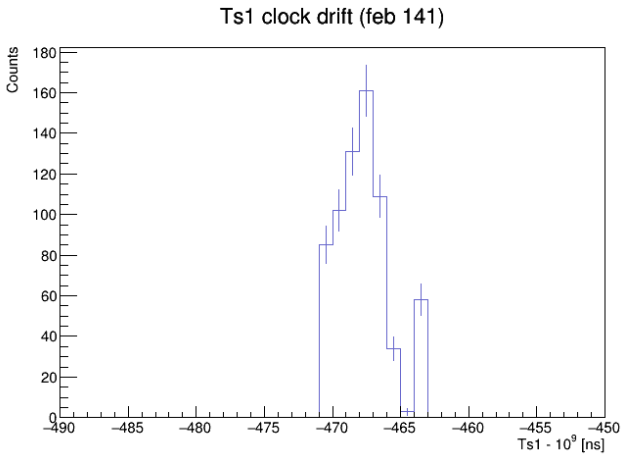
Ts1 clock drift (feb 141)
Counts
Ts1 - 10^9 [ns]

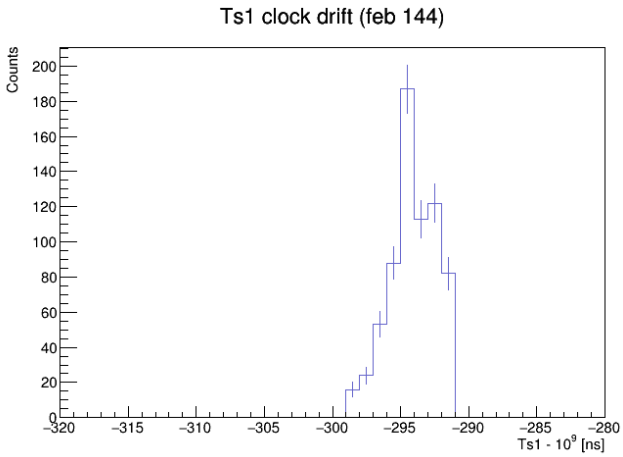
Ts1 clock drift (feb 144)
Counts
Ts1 - 10^9 [ns]

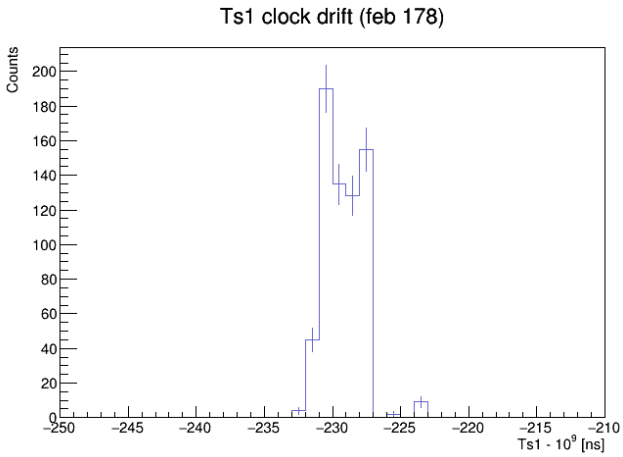
Ts1 clock drift (feb 178)
Counts
Ts1 - 10^9 [ns]

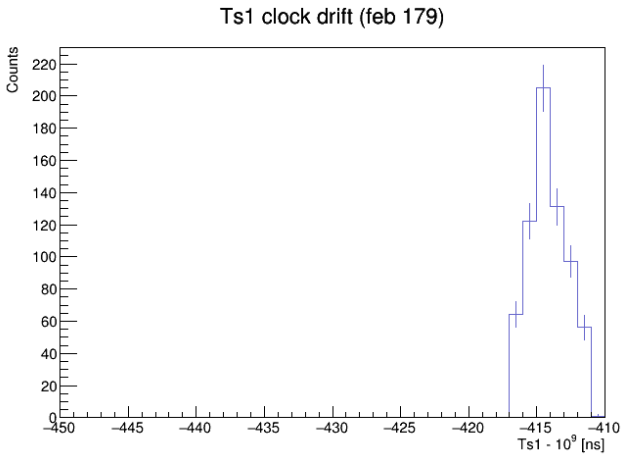
Ts1 clock drift (feb 179)
Counts
Ts1 - 10^9 [ns]

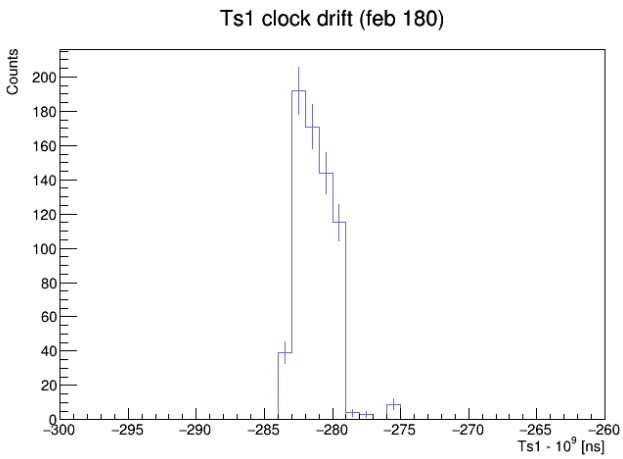
Ts1 clock drift (feb 180)
Counts
Ts1 - 10^9 [ns]

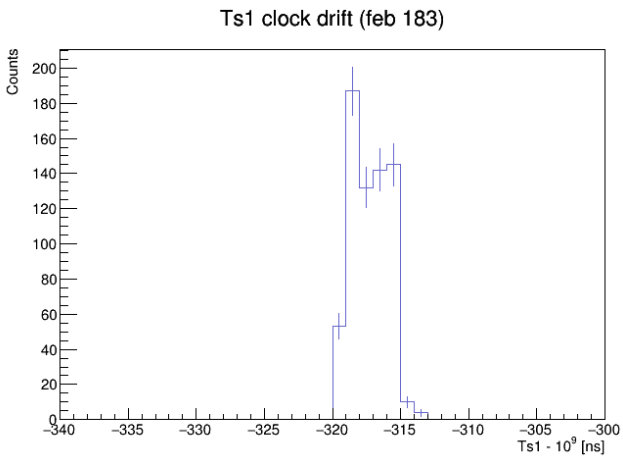
Ts1 clock drift (feb 183)
Counts
Ts1 - 10^9 [ns]

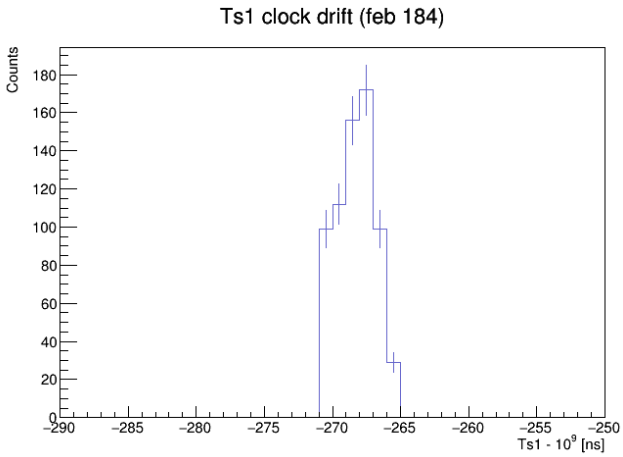
Ts1 clock drift (feb 184)
Counts
Ts1 - 10^9 [ns]

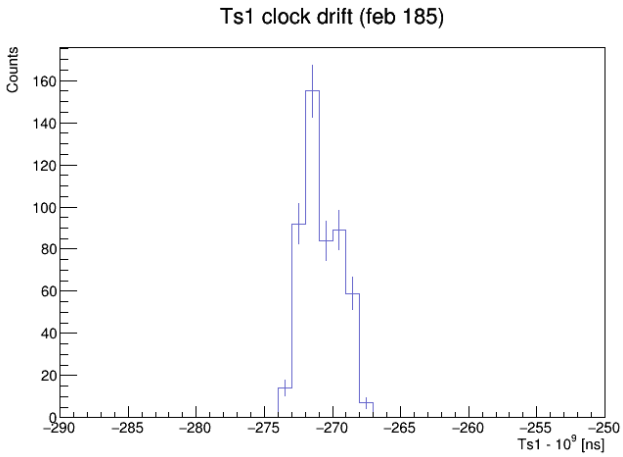
Ts1 clock drift (feb 185)
Counts
Ts1 - 10^9 [ns]

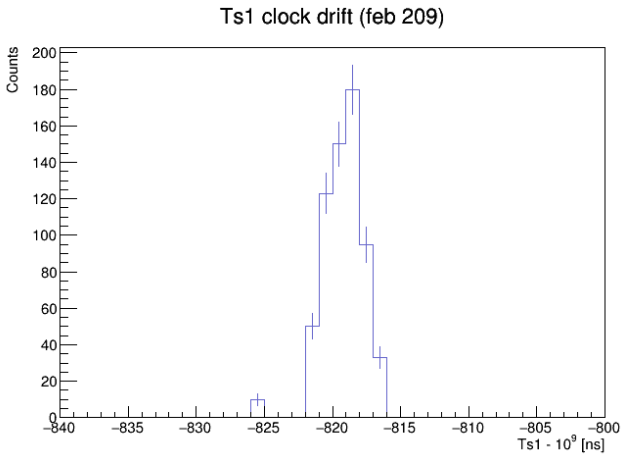
Ts1 clock drift (feb 209)
Counts
Ts1 - 10^9 [ns]

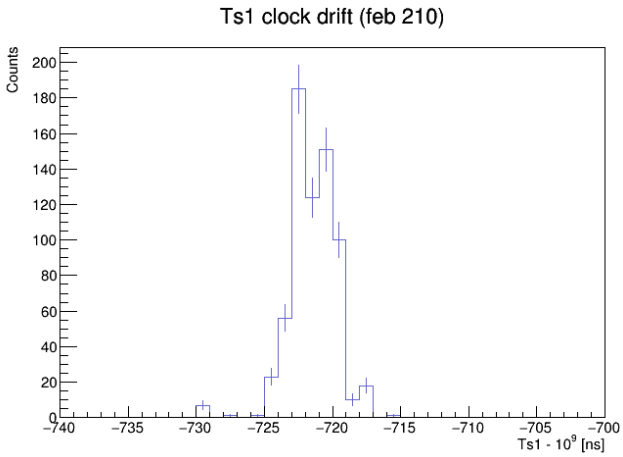
Ts1 clock drift (feb 210)
Counts
Ts1 - 10^9 [ns]

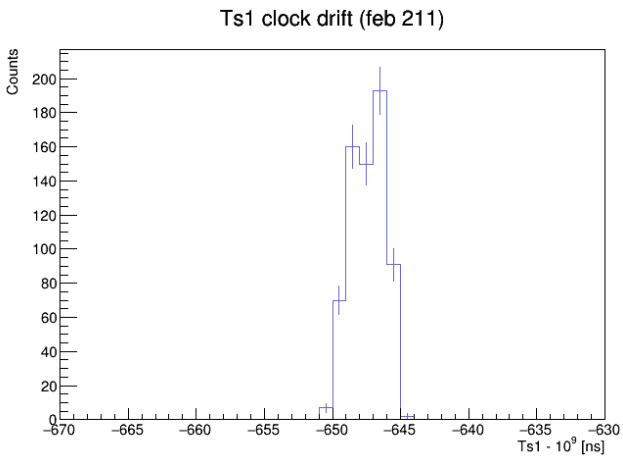
Ts1 clock drift (feb 211)
Counts
Ts1 - 10^9 [ns]

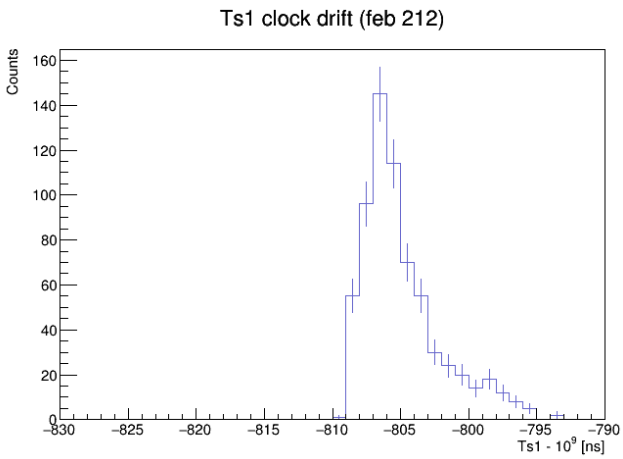
Ts1 clock drift (feb 212)
Counts
Ts1 - 10^9 [ns]

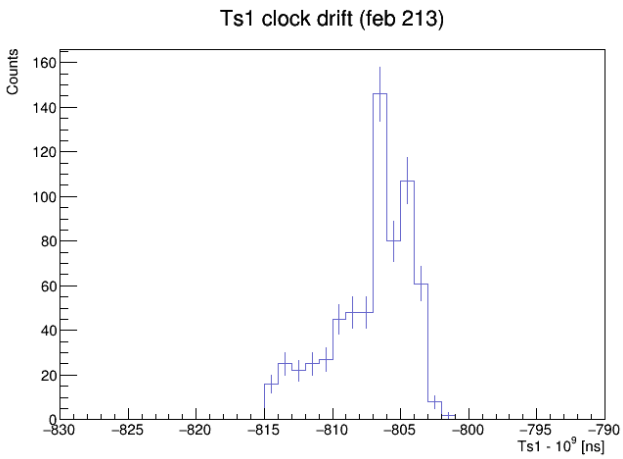
Ts1 clock drift (feb 213)
Counts
160
140
120
100
80
60
40
20
0
−830
−825
−820
−815
−810
−805
−800
−795
−790
Ts1 - 10^9 [ns]

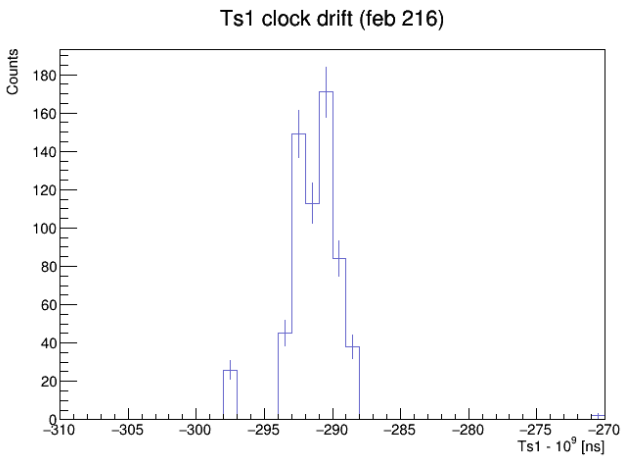
Ts1 clock drift (feb 216)
Counts
180
160
140
120
100
80
60
40
20
0
−310
−305
−300
−295
−290
−285
−280
−275
−270
Ts1 - 10^9 [ns]

B.2 Run 16906

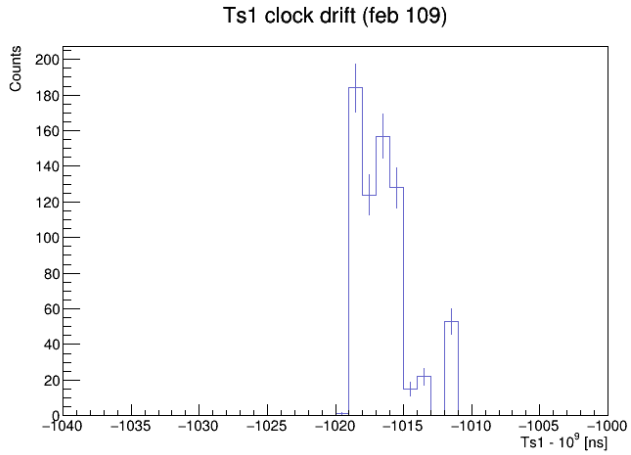
Ts1 clock drift (feb 109)
Counts
Ts1 - 10^9 [ns]

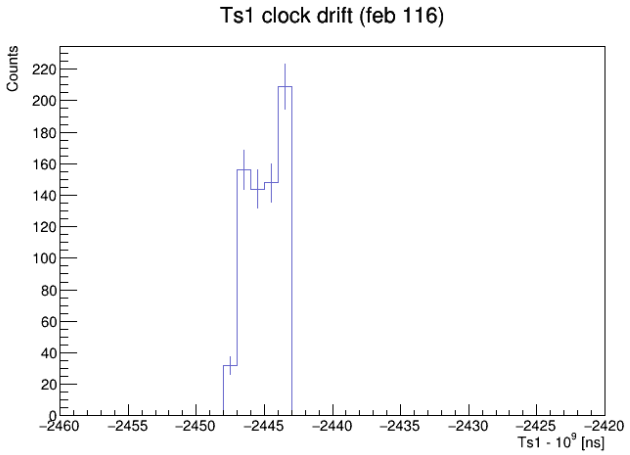
Ts1 clock drift (feb 116)
Counts
Ts1 - 10^9 [ns]

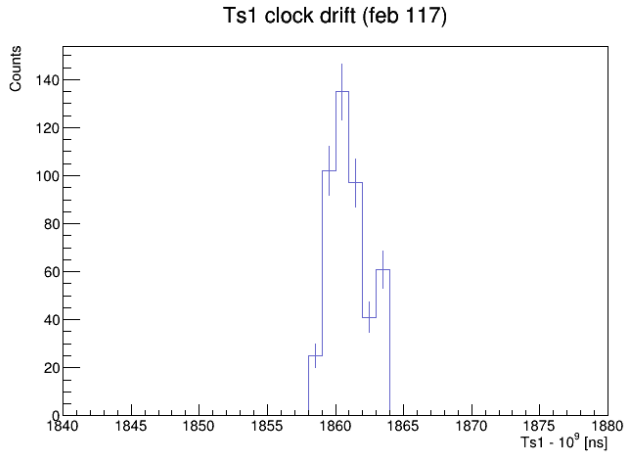
Ts1 clock drift (feb 117)
Counts
Ts1 - 10^9 [ns]

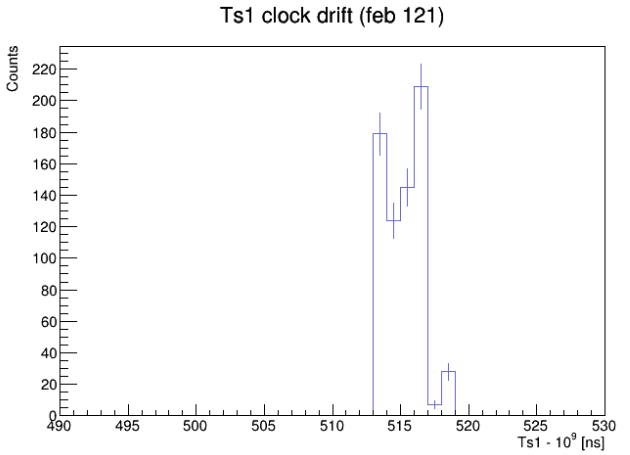
Ts1 clock drift (feb 121)
Counts
Ts1 - 10^9 [ns]

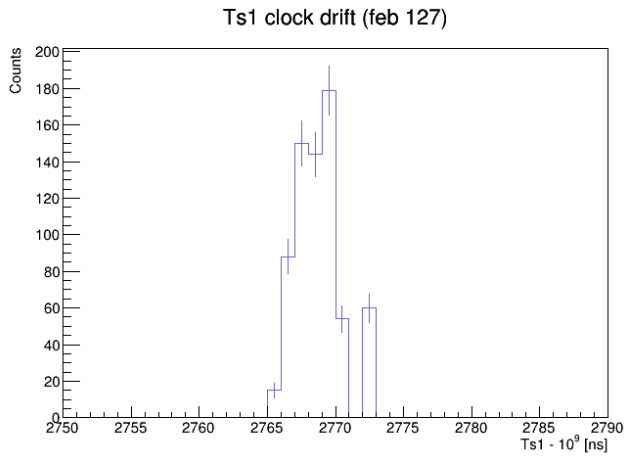
Ts1 clock drift (feb 127)
Counts
Ts1 - 10^9 [ns]

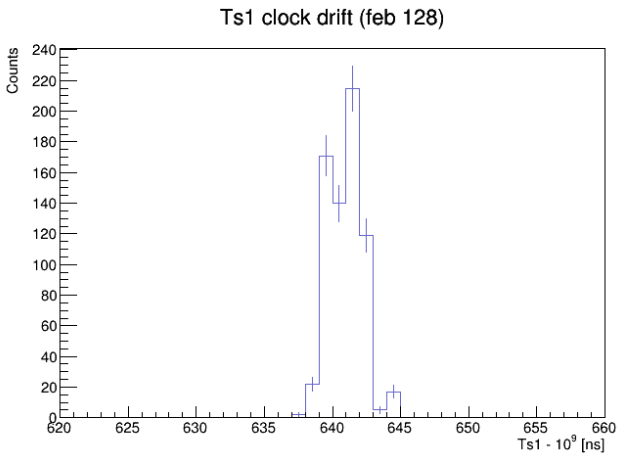
Ts1 clock drift (feb 128)
Counts
Ts1 - 10^9 [ns]

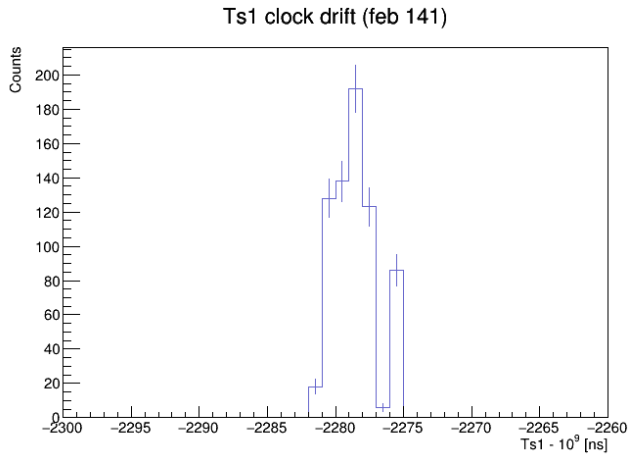
Ts1 clock drift (feb 141)
Counts
Ts1 - 10^9 [ns]

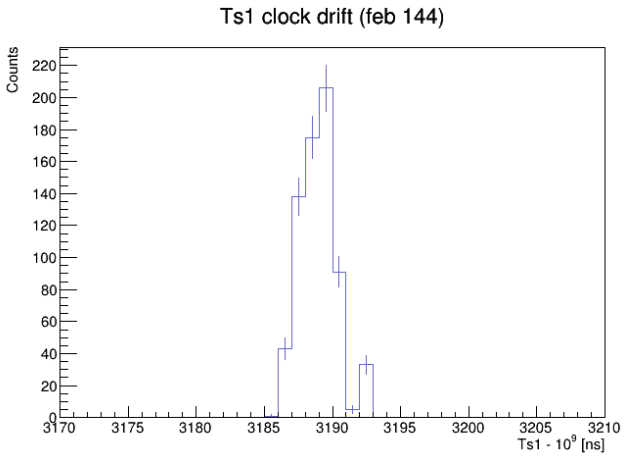
Ts1 clock drift (feb 144)
Counts
Ts1 - 10^9 [ns]

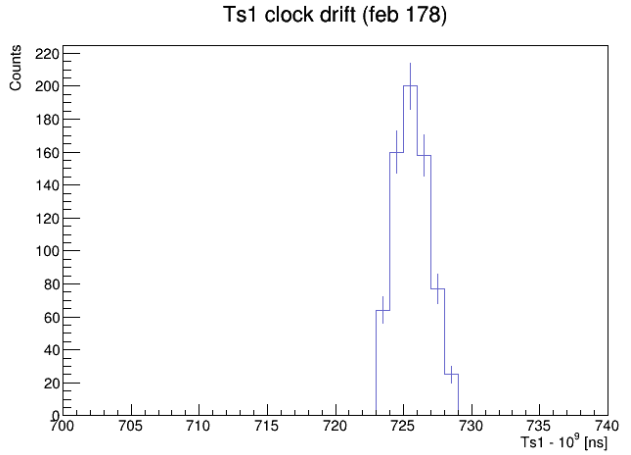
Ts1 clock drift (feb 178)
Counts
Ts1 - 10^9 [ns]

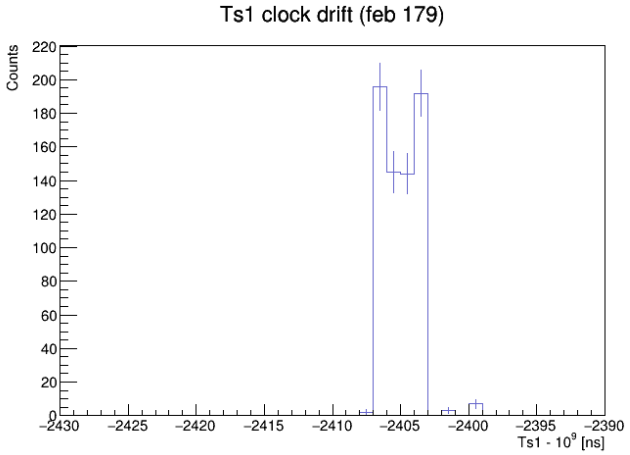
Ts1 clock drift (feb 179)
Counts
Ts1 - 10^9 [ns]

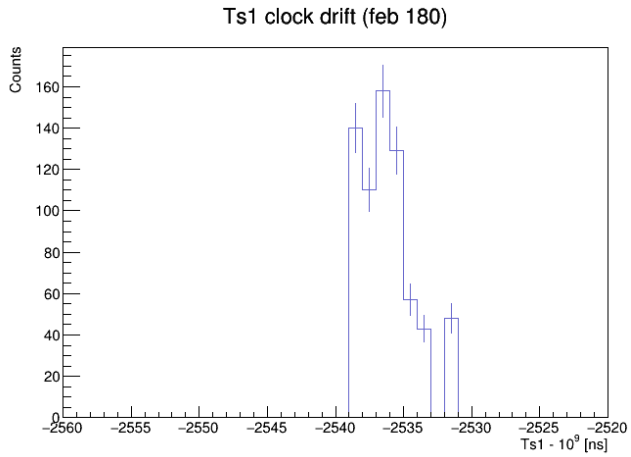
Ts1 clock drift (feb 180)
Counts
Ts1 - 10^9 [ns]

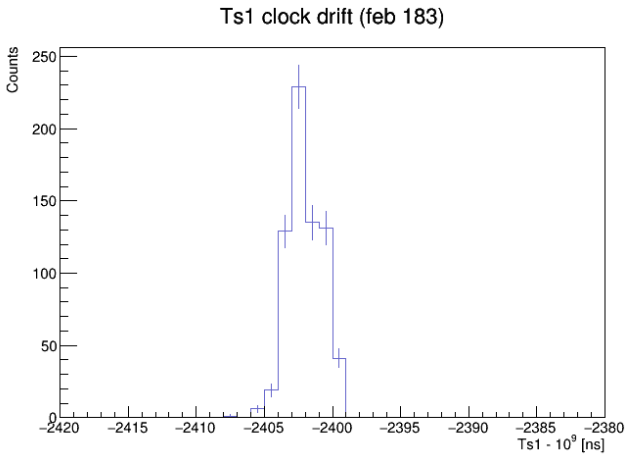
Ts1 clock drift (feb 183)
Counts
Ts1 - 10^9 [ns]

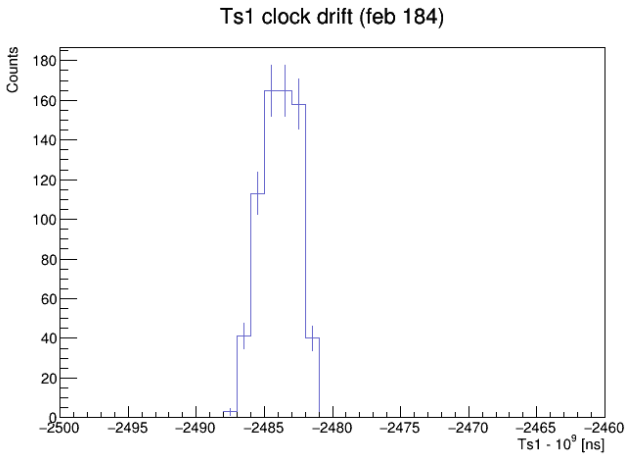
Ts1 clock drift (feb 184)
Counts
Ts1 - 10^9 [ns]

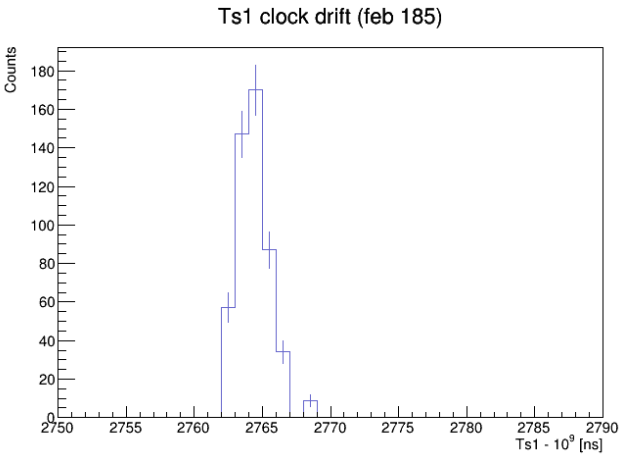
Ts1 clock drift (feb 185)
Counts
Ts1 - 10^9 [ns]

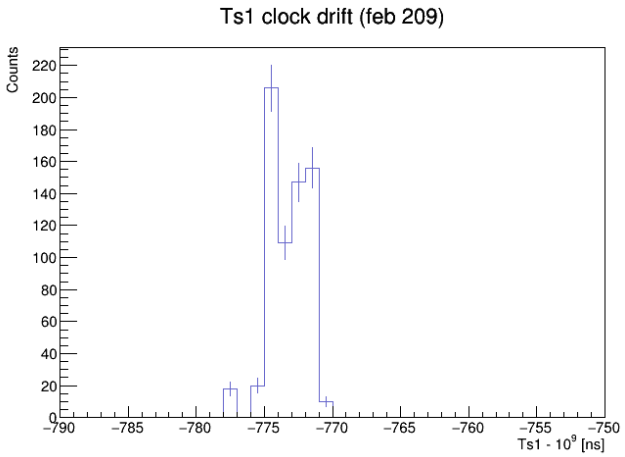
Ts1 clock drift (feb 209)
Counts
Ts1 - 10^9 [ns]

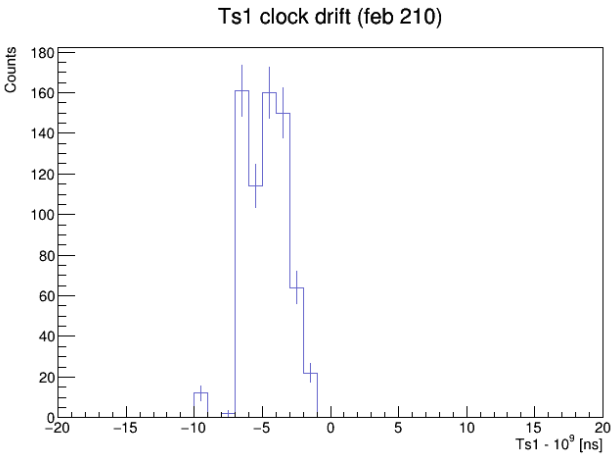
Ts1 clock drift (feb 210)
Counts
Ts1 - 10^9 [ns]

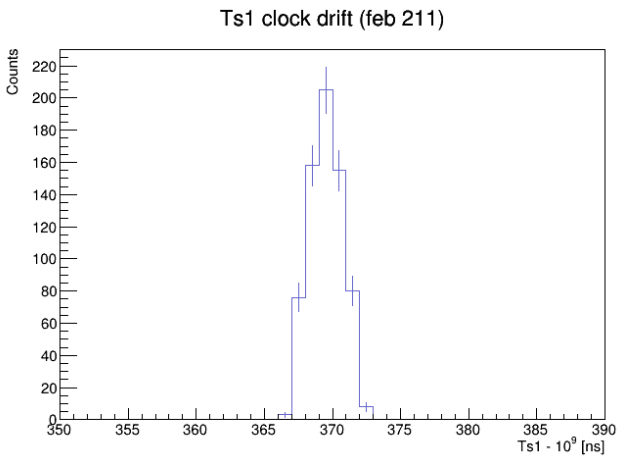
Ts1 clock drift (feb 211)
Counts
Ts1 - 10^9 [ns]

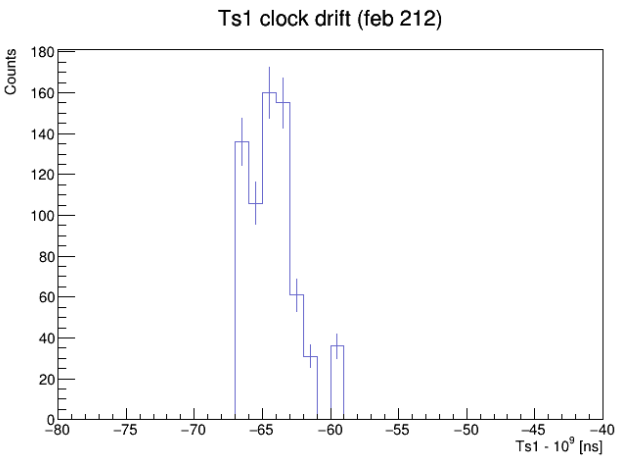
Ts1 clock drift (feb 212)
Counts
Ts1 - 10^9 [ns]

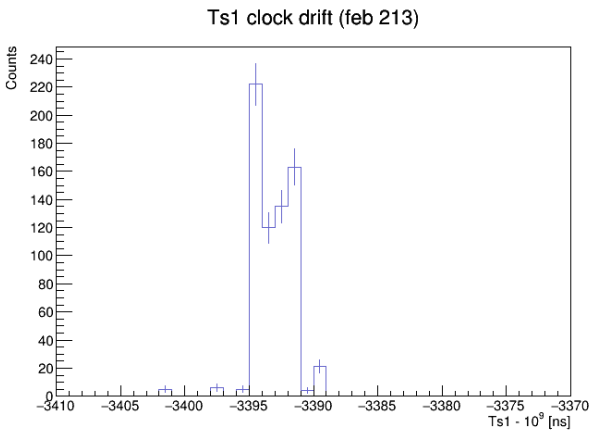
Ts1 clock drift (feb 213)
Counts
Ts1 - 10^9 [ns]

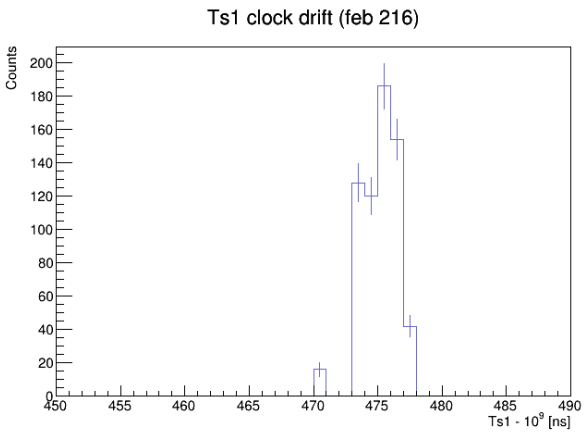
Ts1 clock drift (feb 216)
Counts
Ts1 - 10^9 [ns]